IJST, Transactions of Civil Engineering, Vol. 37, No. C1, pp 77-95
Printed in The Islamic Republic of Iran, 2013

NUMERICAL SIMULATION OF FREE SURFACE MUDFLOW USING INCOMPRESSIBLE SPH*

Z. GHADAMPOUR[1**], N. TALEBBEYDOKHTI[2], M. R. HASHEMI[3], A. H. NIKSERESHT[4] AND S. P. NEILL[5]

[1]Dept. of Civil and Environmental Engineering, Shiraz University, I. R. of Iran
Email: Zahra_ghadampour@yahoo.com
[2]Dept. of Civil and Environmental Engineering, Environmental Research and Sustainable Development Center, Shiraz University, I. R. of Iran
[3]Dept. of Water Engineering, Shiraz University, I. R. of Iran; School of Ocean Sciences, Bangor University, Menai Bridge, UK
[4]Dept. of Mechanical Engineering, Shiraz University of Technology, I. R. of Iran
[5]School of Ocean Sciences, Bangor University, Menai Bridge, UK

Abstract– In this paper, Incompressible SPH (ISPH) is used to simulate free-surface mudflow for two case studies, including dambreak and flow under a gate. The mixture of water and sediment in mudflow is treated as a non-Newtonian fluid. Mass and momentum conservation equations in a 2-D Lagrangian frame, along with the Herschel-Bulkley rheology model, were solved to simulate mudflow using ISPH. Further, a Large Eddy Simulation (LES) model was used to evaluate the effect of turbulence on the free surface flow for these cases. The divergence-free velocity projection method was applied to enforce incompressibility of SPH. The results of the ISPH modeling compared well with experimental data and FVM-VOF results. The capability of the ISPH Lagrangian numerical model to capture large deformations makes it a powerful and efficient method for simulating mudflow case studies.

Keywords– ISPH, gate, hydraulic jump, dambreak, mudflow, multi-phase flow

1. INTRODUCTION

Mudflow is a type of hyper-concentrated sediment flow that is characterized by high concentrations of silt and clay [1]. There are numerous causes which initiate these flows, including intense rainfall, submarine landslides, dambreak on sloping beds, and anthropogenic activities. Multi-phase flow, highly viscous fluids, sediment transport, unknown mudflow waterfront properties, undetermined fluid mixture viscosity, and turbulent characteristics are some of the complicating features of mudflow. Mudflow can lead to major damages to river protection structures and other hydraulic structures [2, 3].

Therefore, the simulation of mudflow is essential to clarify the flow impact on the design and operation of hydraulic structures in order to reduce destructive effects.

Traditionally, experimental methods have been used to predict mudflow behavior [4, 5], however, measurement error, cost, and scale effects are some of the disadvantages of such methods. Nevertheless, fluid mixture rheological properties such as mixing, density, and sediment percentages have been determined by experimental methods up until now. With recent advances in computational power, mathematical models are now more widely used to model mudflow in one, two, and three dimensions [6].

*Received by the editors July 1, 2012; Accepted December 4, 2012.
**Corresponding author

Until now, two main mathematical approaches have been used to describe multi-phase free surface flows such as mudflow [7]. In the first method, which is the most common, separate equations are used to simulate solid (sediment) and liquid (water) phases. Usually, the continuity and momentum equations are used to model the fluid phase, and an advection-diffusion model is used to simulate the sediment transport [8, 9]. However, this method suffers from some difficulties such as considerable computational effort required to solve the coupled equations.

In the second method, the water/sediment mixture is treated as a non-Newtonian fluid, in which the relation between shear stress and rate of shear strain is nonlinear. Thus, in the second method, there is no need to consider the role of pore pressure distribution and localized surface tension, and a single set of equations with a non-Newtonian model, used to calculate nonlinear viscosity, is implemented to simulate the behavior of a mudflow system [10, 11]. The appropriate non-Newtonian model and numerical method to solve mudflow equations are two main issues that must be considered in simulating free surface mudflow.

Viscoplastic models are non-Newtonian fluids which are commonly used as a model to describe the viscosity of natural gravity-driven mudflow. Different constitutive equations of viscoplastic model such as cross, Bingham plastic, Herschel-Bulkley, and generalized viscoplastic models are used to describe the relatively complex rheology of mudflow [12-14]. Apparent viscosity is evaluated in all of these models, and is implemented in mathematical equations of free surface flow, typically the Navier-Stokes equation, instead of dynamic viscosity. This strategy makes it possible to model different types of flow such as mudflow.

In various applications regarding the rheological properties derived from different experimental data it has been shown that the Herschel-Bulkley model is an appropriate model to describe the properties of mudflow [15].

Numerical methods which solve free surface mudflow equations can be classified into mesh-based and mesh-free categories. In order to overcome some difficulties and limitations that are associated with traditional mesh-based methods, novel numerical methods, namely mesh-free methods, have been gradually applied to different areas of fluid mechanics, particularly free surface problems [16]. Smoothed particle hydrodynamics (SPH) is one of the most powerful mesh-free methods that has recently been used to simulate free-surface flow problems [17]. SPH was originally developed in the late 1970s for astrophysical applications [18, 19], and was later applied to solid mechanics [20]. The ability of SPH in capturing large deformations led to its subsequent application to simulating free surface flows.

SPH was firstly employed in free surface flows to model wave breaking [21], and progressively extended into other free surface applications. It has been used to successfully simulate some multi-phase free-surface flow problems such non-Newtonian dambreak on a horizontal bed [14], dambreak for mudflow down a steep flume [22], mobile-bed dambreak [7], landslides and debris flow [23], wave interactions with porous media [24], rapid sediment scour [25], the lock-exchange problem [26], granular free surface flow [27], and scouring beneath marine pipelines [28].

Many advantages have been reported in the application of SPH to the above problems. Firstly, easy tracking of the free surface, which is a challenge for Eulerian methods. Secondly, a Lagrangian description of flow particles can be useful when simulating highly transitory mudflow problems. Finally, the numerical formulation of SPH and consideration of the constitutive equation of a non-Newtonian fluid is relatively easy, compared to mesh-based methods.

However, the implementation of solid boundary conditions is not straightforward in SPH, and the method requires considerable computational effort. Since SPH was originally formulated for compressible flows, its application to incompressible flows (e.g. simulating mudflow) is a more challenging task, and

the subject of much debate. In addition, due to the difficulty of satisfying boundary conditions in most turbulence models, it is not easy to apply these models in SPH. Recently, some advances have been achieved to overcome these major drawbacks and complexities in SPH.

To enforce incompressibility, weakly compressible (WCSPH) and fully incompressible versions of SPH have been proposed, and compared to each other for modeling incompressible free-surface flows [29, 30]. Incompressible flow is considered as a weakly compressible flow in WCSPH, and the pressure is calculated using the equation of state. Although WCSPH is relatively simple to program, due to some drawbacks such as pressure fluctuations, incompressible SPH has been introduced gradually into free surface flow problems [29, 31]. Generally, incompressibility is enforced in ISPH by solving the Poisson equation, based on two projection methods: divergence-free velocity and density-invariant [32, 33]. However, few non-Newtonian problems such as dam break analysis and mild-slope are simulated using the projection method [14]. Therefore, more research is required to evaluate the performance of ISPH in mudflow problems.

Another important issue that hyper-concentrated fluids such as mudflow may encounter is turbulence, which can generally be modeled based on two approaches: using different laminarization methods, and direct numerical simulation (DNS). Although no modeling is required in DNS, and the turbulent energy cascade is resolved directly, it is still not applied in SPH due to its high computational cost [34]. Over the last decade, turbulence modeling for incompressible free surface problems is gradually emerging into SPH, based on time averaging or filtering of the Navier-Stokes equations. Although turbulence modeling is not used in mudflow problems, it has been applied to several free surface flow problems. The algebraic mixing length equation, the simplest of all turbulence models, is based on the Boussinesq eddy-viscosity approximation, and has been successfully applied to free surface flow problems [35]. The two equation (k-ε) model was also implemented in SPH based on the Reynolds averaged Navier-Stokes (RANS) to model wave breaking and dambreak. Although the standard k-ε model provided satisfactory results for turbulent isotropic flow, it is not appropriate for more complex free surface problems such as low-Reynolds flow, and flow near boundaries. Further, implementation of the boundary condition is not straightforward in the k-ε model [36]. Explicit Algebraic Reynolds Stress Models (EARSM) are in the category of turbulence models based on the Reynolds averaged idea, and have been applied to simulate the collapse of water in SPH. To compare with the former method, EARSM generally covers the disadvantages of the k-ε model [37]. However, solving five equations simultaneously in 2-D, while satisfying the B.C. for all of them, is a difficult and time consuming task. In addition, stability of the model is sensitive to the computational grid and B.C. Another alternative to simulating turbulence is large eddy simulation (LES), which is one of the most popular turbulence models in SPH. The time-dependent Navier-Stokes equations are averaged by filtering in Fourier or physical space. Therefore, the dynamics of large eddies in the turbulent energy cascade can be modeled directly. LES has been applied successfully in several free surface problems such as dambreak, wave breaking, and solitary waves in SPH and ISPH [33, 38, 39, 40]. Further, 3D water column collapse, water wave, and sloshing problems have been simulated using LES in SPH [41, 42]. Due to the relatively simple representation of the B.C. and accurate results of LES, it has been applied more than any of the other turbulence models in simulating free surface flow.

In summary, despite the powerful performance of SPH in simulating complicated flows, there have been few attempts to apply ISPH to mudflow problems. Additionally, while turbulence modeling is commonly used in simulating free surface flows, it has not yet been applied to mudflow problems.

The aim of this paper is to apply ISPH to some mudflow problems and evaluate the efficiency of this powerful method in simulating such flows. Due to high computational cost, we apply the method to solve small scale problems in the present study. Several cases such as flow under a gate with different downstream conditions, dam break, and submarine mudflow are examined. Incompressibility is enforced

using the divergence-free velocity projection method, and the Herschel-Bulkley rheological equation is used to model mudflow properties. We investigate the effect of the LES laminarization model in reproducing turbulence effects of mudflow in ISPH, and several bench marks, including FVM-VOF and experimental data, are used to verify the ISPH results.

2. GOVERNING EQUATIONS

The continuity and momentum equations in a 2-D Lagrangian frame were used to simulate free-surface mudflow [43]

$$\frac{1}{\rho}\frac{D\rho}{Dt} + \nabla.(\vec{V}) = 0 \tag{1}$$

$$\frac{D\vec{V}}{Dt} = -\frac{\nabla P}{\rho} + \vec{g} + \frac{1}{\rho}\nabla.\tilde{\tau} \tag{2}$$

where $V = 2$-D velocity vector, $P =$ pressure, $\rho =$ fluid density, $g =$ gravitational acceleration vector, $t =$ time and $\tilde{\tau} =$ SGS shear stress tensor in the LES anisotropic turbulence model, which is related to the resolved strain rate tensor as,

$$\frac{\tau_{SGS}}{\rho} = 2(\upsilon_{app} + \upsilon_t)\tilde{S}_{ij} - \frac{2}{3}k\delta_{ij} \tag{3}$$

where $\upsilon_{app} =$ molecular viscosity for water or apparent viscosity for mudflow, $\upsilon_t =$ turbulent eddy viscosity, $k =$ SGS turbulent kinetic energy, $\delta_{ij} =$ Kronecker delta, and $\tilde{S}_{ij} =$ SGS strain rate tensor which is defined as,

$$\tilde{S}_{ij} = \frac{1}{2}\left(\frac{\partial V_i}{\partial x_j} + \frac{\partial V_j}{\partial x_i}\right) \tag{4}$$

For incompressible flow, the second term in Eq. (3) is omitted. The most widely used and the simplest model to define υ_s was proposed by Smogorinskey as,

$$\upsilon_s = l_s^2\left(2\bar{S}_{ij}\bar{S}_{ij}\right)^{\frac{1}{2}} \tag{5}$$

where $l_s =$ the mixing length for subgrid scale and is computed as

$$l_s = C_s^2\left(\Delta x \Delta y\right) \tag{6}$$

where $C_s =$ Smogoriskey constant which is in the range of 0.094-0.2 [38] . For free surface flow in regions far from the wall, this constant is close to the value 0.1, and for the region near the wall it is calculated using,

$$C_s = 0.1\left\{1.0 - \exp\left[\left(-\frac{y_t}{25}\right)^3\right]\right\} \tag{7}$$

in which

$$y_t = \frac{y}{u_* / \upsilon} \ , \ u_* = \sqrt{\frac{\tau_w}{\rho}}$$

where $y =$ distance to the wall and $u_* =$ shear velocity.
To evaluate the turbulence intensity, the turbulence parameter is defined as

$$T.P = \frac{\mu_t}{\mu} \tag{8}$$

where μ_t and μ are dynamic turbulence and molecular viscosity, respectively.

3. SPH FORMULATION OF FREE SURFACE MUDFLOW

The mathematical equations are solved based on the predictor-corrector scheme using SPH. Details regarding SPH are described in the following sections.

a) Introduction to SPH

SPH is a Lagrangian numerical method, in which the computational domain is represented by particles without any connectivity between them. The interpolation process of any field function $f(x)$ in a discrete manner can be represented as,

$$\langle f(x) \rangle = \sum_{j=1}^{N} \frac{m_j}{\rho_j} f(x_j) W(x - x_j, h) dx' \tag{9}$$

where $x = (x, y)$ is the position vector, x' is a dummy variable, h is a smoothing length, and the summation is performed over all of the particles inside the support domain. The kernel function W is determined according to some basic properties such as unity, compact support, isotropy, oddness, positivity, and uniform smoothness [16]. Among various expressions that have been introduced in the literature, the B-Spline kernel function is the most commonly used for free surface problems and is therefore used in this research:

$$\begin{cases} W(r,h) = \frac{10}{7\pi h^2}(1 - \frac{3}{2}R^2 + \frac{3}{4}R^3) & R < 1 \\ W(r,h) = \frac{10}{28\pi h^2}(2 - R)^3 & 1 \le R \le 2 \\ W(r,h) = 0 & R > 2 \end{cases} \tag{10}$$

where $R = \frac{r}{h}$ and r is the distance between two particles.
Referring to Eq. (9), fluid density for particle i is,

$$\rho_i = \sum_{j=1}^{N} \frac{m_j}{\rho_j} f(\mathrm{x}_j) W(\mathrm{x}_i - \mathrm{x}_j, h) d\mathrm{x}' \tag{11}$$

where ρ_j and m_j, respectively, denote the density and mass of mudflow particles. A more detailed explanation of SPH is presented elsewhere [16, 44]. In the next section, the method for imposing incompressibility in SPH for free-surface problems is discussed.

b) Divergence-free velocity projection method

One of the main approaches for imposing incompressibility in SPH is the divergence-free velocity method.

In this method, the position and velocity of particles in the predictor step are computed using [26],

$$\vec{r}_* = \vec{r}_t + \vec{V}_t \Delta t \tag{12}$$

$$\vec{V}_* = \vec{V}_t + \Delta \vec{V}_* \tag{13}$$

where subscripts t and * represent the variables at time t, and at the predictor step, respectively. Also, ΔV_* is given by,

$$\Delta \vec{V}_* = \left(\bar{g} + \frac{1}{\rho} \nabla . \tilde{\tau} \right) \Delta t \tag{14}$$

Therefore, r_* is used to evaluate ρ_* (Eq. (11)), and V_* is replaced in the source term of the Poisson equation to update the pressure at $t+1$ as follows [32],

$$\nabla . \left(\frac{1}{\rho_*} \nabla P_{t+1} \right) = \frac{\nabla . \vec{V}_*}{\Delta t} \tag{15}$$

In the corrector step, P_{t+1} is used to calculate the position and velocity of particles at $t+1$,

$$\vec{V}_{t+1} = \vec{V}_* + \Delta \vec{V}_{**} \tag{16}$$

$$\vec{r}_{t+1} = \vec{r}_t + \frac{\vec{V}_t + \vec{V}_{t+1}}{2} \Delta t \tag{17}$$

where ΔV_{**} is,

$$\Delta \vec{V}_{**} = -\frac{1}{\rho_*} \nabla P_{t+1} \Delta t \tag{18}$$

1- SPH approximation of various terms in the projection method: Divergence, Laplacian, and gradient operators that have been used in the formulations of the projection method should be expanded using SPH rules.

The divergence operator has been defined in various ways in previous SPH studies but, according to Liu [44], the following relation can improve the accuracy of the numerical method for the velocity term, and is used to define the RHS of the Poisson Equation,

$$\frac{\nabla . \vec{V}_*}{\Delta t} = \frac{\frac{1}{\rho} \sum_{j=1}^{N} m_j (\vec{V}_i - \vec{V}_j) . \nabla_i W_{ij}}{\Delta t} \tag{19}$$

in which,

$$\nabla_i W_{ij} = \left(\frac{\partial W_{ij}}{\partial r_{ij}} \left(\frac{x_i - x_j}{r_{ij}} \right), \frac{\partial W_{ij}}{\partial r_{ij}} \left(\frac{y_i - y_j}{r_{ij}} \right) \right) \tag{20}$$

The LHS of the Poisson Equation (Laplacian term) can also be approximated using different SPH formulations. One of the most popular equations is defined here by the following relationship,

$$\nabla.\left(\frac{1}{\rho}\nabla P\right)_i = \sum_{j=1}^{N} m_j \frac{8}{(\rho_i+\rho_j)^2}\frac{P_{ij}\vec{r}_{ij}.\nabla_i W_{ij}}{\left|\vec{r}_{ij}\right|^2+\eta^2} \tag{21}$$

where η is a constant to prevent the denominator becoming zero during the computation, and is usually taken as $0.1h$ [24].

The gradient operator that has been used in Eq. (2) can be replaced in SPH using,

$$\left(\frac{1}{\rho}\nabla P\right)_i = \sum_j m_j\left(\frac{P_i}{\rho_i^2}+\frac{P_j}{\rho_j^2}\right)\nabla_i W_{ij} \tag{22}$$

The viscosity term in Eq. (2) is represented in SPH as,

$$\frac{1}{\rho}\nabla.\tilde{\tau} = \sum_j m_j\left(\frac{\tilde{\tau}_i}{\rho_i^2}+\frac{\tilde{\tau}_j}{\rho_j^2}\right).\nabla_i W_{ij} \tag{23}$$

where $\tilde{\tau}$ is related to the rate of strain according to Eq. (3). To evaluate $\tilde{S}_{ij}$ in SPH, $\frac{\partial u_i}{\partial x_j}$ in Eq. (4) may be approximated by

$$\left(\frac{\partial u_i}{\partial x_j}\right) = \left(\frac{\partial u_i}{\partial r}\right)\left(\frac{\partial r}{\partial x_j}\right) \tag{24}$$

in which i , j are dummy indices in x and y directions.

c) Rheological model

Slurries composed of a mixture of kaolin and water are usually considered to behave like non-Newtonian mudflows. Experimental results show that in the majority of problems, the Herschel-Bulkley model can correctly describe the nonlinear properties of the stress tensor in mudflow [45]. In summary, the model is a combination of the power law and Bingham models, in which the stress for describing the nonlinear viscoplastic behavior of mudflow is defined as

$$\tau = \begin{cases} 0 & \tau \prec \tau_B \\ \tau_B + \mu_B(\dot{\gamma})^N & \tau \succeq \tau_B \end{cases} \tag{25}$$

where τ_B, μ_B, and N are yield stress, equivalent dynamic viscosity, and flow behavior index, respectively. These two final parameters are usually determined based on experimental viscometer results. The shear strain rate ($\dot{\gamma}$) is given in 2-D,

$$\dot{\gamma} = (2S_{ij}S_{ij})^{\frac{1}{2}} = \sqrt{2\left(\frac{\partial u}{\partial x}\right)^2+2\left(\frac{\partial v}{\partial y}\right)^2+\left(\frac{\partial u}{\partial y}+\frac{\partial v}{\partial x}\right)^2} \tag{26}$$

The velocity gradient terms used in the calculation of shear may be approximated in SPH using Eq. (24). Accordingly, the apparent viscosity for mudflow in the Herschel-Bulkley model is defined as

$$\mu_{app} = \frac{\tau_B}{\dot{\gamma}} + \mu_B(\dot{\gamma})^{N-1} \tag{27}$$

The above-mentioned term is replaced in Eq. (3) to determine shear stress in the turbulence model.

d) Error estimation

Normal density error at each time step is used as a criterion to estimate the error of the projection methods. It is expressed as,

$$E_d(t) = \frac{1}{N'}\sum_{i=1}^{N'}\left(\frac{|\rho_i(t) - \rho_0|}{\rho_0}\right) \tag{28}$$

where ρ_i is the particle density at each time step, ρ_0 is the initial particle density, and N' is the number of fluid particles.

4. MODEL APPLICATIONS AND RESULTS

To evaluate performance, the ISPH method was applied to several case studies: dambreak with a dry downstream mild bed, flow under a gate with downstream tail water, and submarine landslide. Various complexities such as rapidly varying flow, non-hydrostatic pressure distribution, turbulent flow, regular and submerged hydraulic jumps, and multiphase flow are features of the selected problems. For comparison of the results, different bench marks, including FVM-VOF and experimental data, were used.

a) Dambreak with downstream mild bed

Dambreak is a complex natural gravity current flow that has been intensively studied, particularly by SPH. While many attempts have been carried out to model Newtonian fluid dambreak [46], viscoplastic material is involved in numerous natural dambreak processes, and few investigations (mainly experimental methods) are reported in this regard.

To model mudflow dambreak problems, the free surface fluid was released instantaneously from behind a lock gate. Different flow profiles may emerge for finite and infinite reservoir extents, as shown in Fig. 1 [47]. The second case (i.e. finite extent) is considered here for the validation of ISPH.

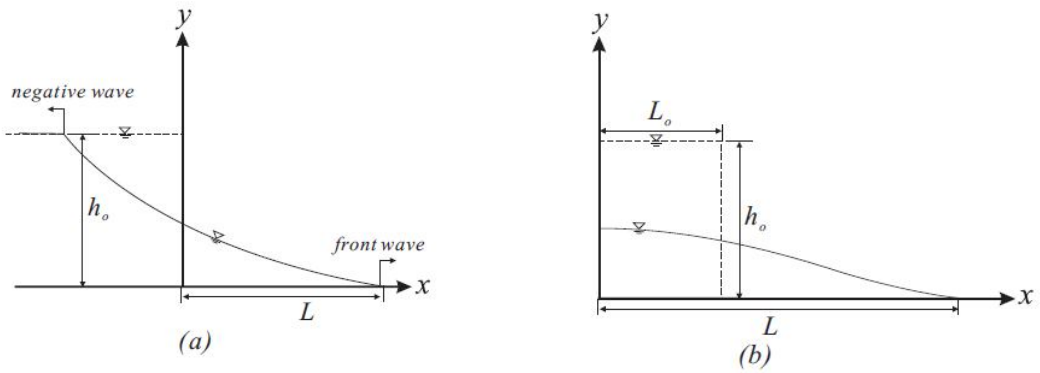

Fig. 1. Dambreak flow of (a) infinite and (b) finite extent [46]

A tank with initial height and length of mudflow equal to 0.11 and 0.5 m, respectively, was considered. The problem is based on water-clay mixture experiments with a volume concentration of 27.4% [48]. The mudflow properties for the Herschel-Bulkley rheological model are shown in Table 1.

Table1. The experimental results of mudflow properties [48]

$\rho\ (kg/m^3)$	$\tau_B\ (Pa)$	$\mu_B\ (\frac{Ns}{m^2})$	K
1200	25.0	0.07	0.5

The results of mudflow modelling based on ISPH numerical methods are shown in Fig. 2. Regarding the stability of ISPH, the time and space intervals were 0.001 s and 0.0045 m, respectively. Details of the computational demand for this problem are reported in Table 2. The ISPH code was run on an AMD Phenom II PC with 3.25 GB of RAM.

The length of the front after dambreak simulated by ISPH at several times is compared with experimental data in Fig. 3. There is good agreement between ISPH and the experimental results [47].

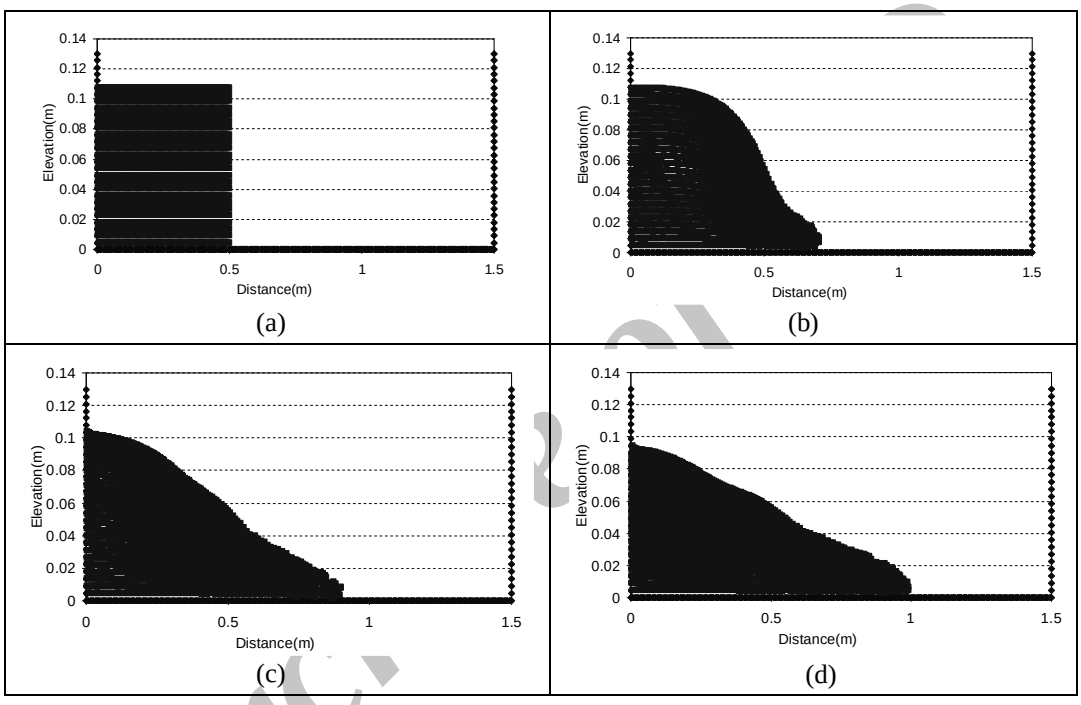

Fig. 2. Free-surface flow after dambreak at times (a) 0 s, (b) 0.2 s, (c) 0.4 s, and (d) 0.6 s using ISPH

Table 2. Computational demand of several problems using ISPH numerical method

Problem	CPU time(s)	No. of iterations	No. of particles
Dambreak	4995	600	3851
Flow under gate (regular hydraulic jump)	1322	200	3476
Flow under gate (submerged hydraulic jump)	1695	200	4052
Submarine landslide	9264	2000	3110

Velocity vectors at various time-scales are shown in Fig. 4. During the initial stages of dambreak, two flow regions may be distinguished. The first region, named subcritical, is characterized by low velocity and high depth, which is in contrast with the second region, named supercritical. The maximum velocity occurs near the bore front in the supercritical region. Due to large deformation of the free surface, a maximum shear rate is also observed near the frontal region.

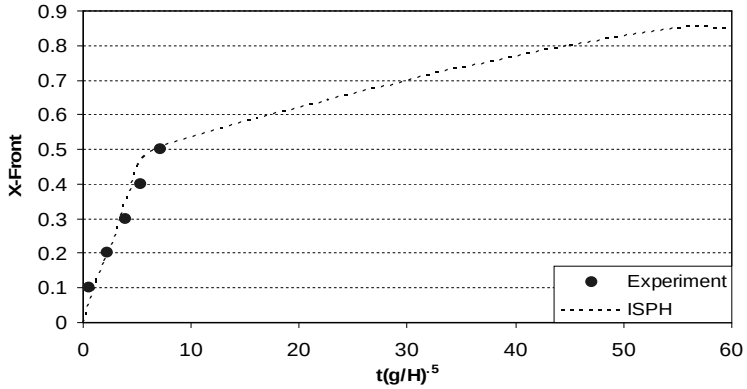

Fig. 3. Comparison of length of front after dambreak, using ISPH, and experimental result

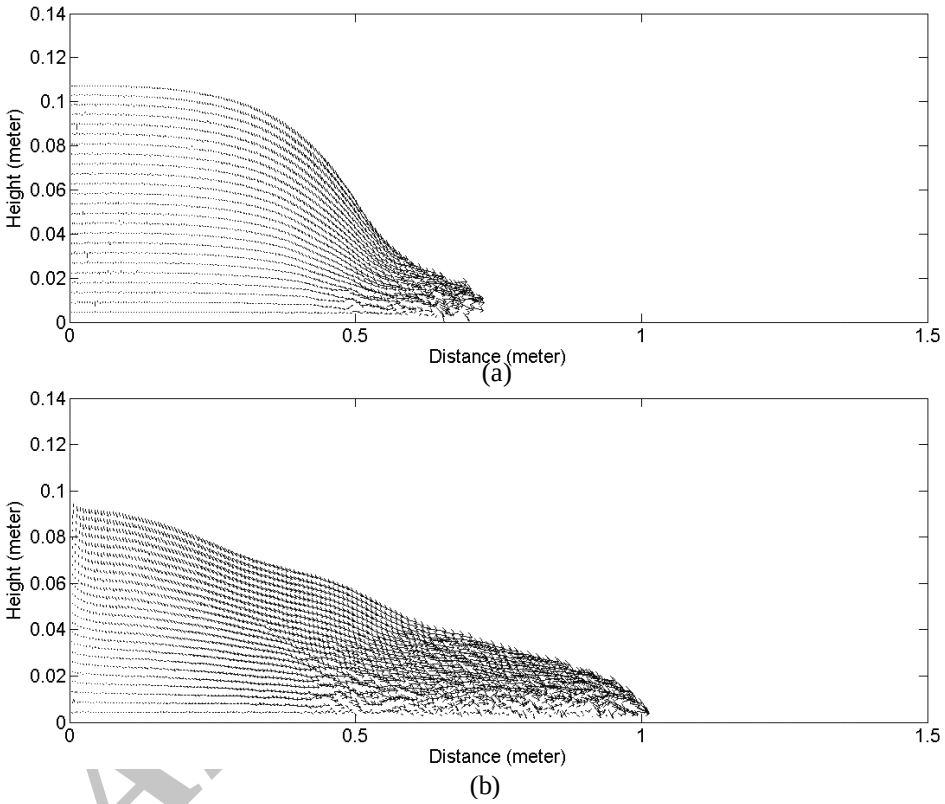

Fig. 4. Velocity vectors after dambreak at times (a) 0.2 s, (b) 0.6 s using ISPH.

Variation of the initial acceleration at the bore front leads to a pressure redistribution (Fig. 5). Over time, the initial acceleration reduces, and the pressure distribution approaches the hydrostatic distribution (after about 0.3 s).

Regarding the effects of turbulence, turbulence parameter fields (Eq. (8)) at two times are shown in Fig. 6. The maximum turbulent intensity is near the bore front, which is affected by a negative wave.

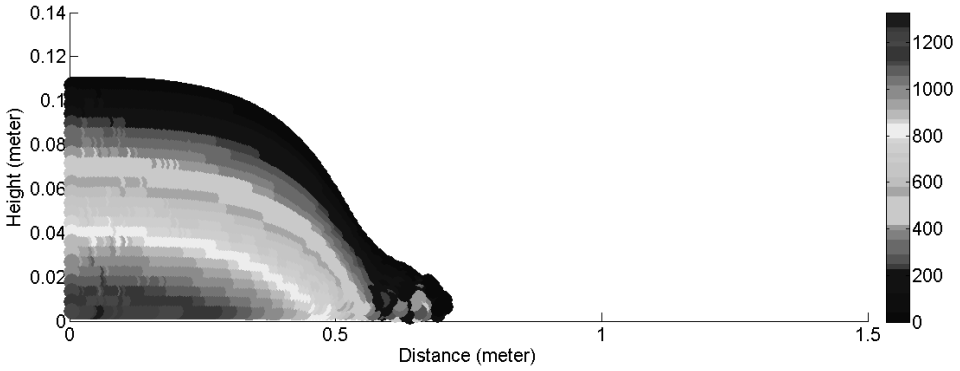

(a)

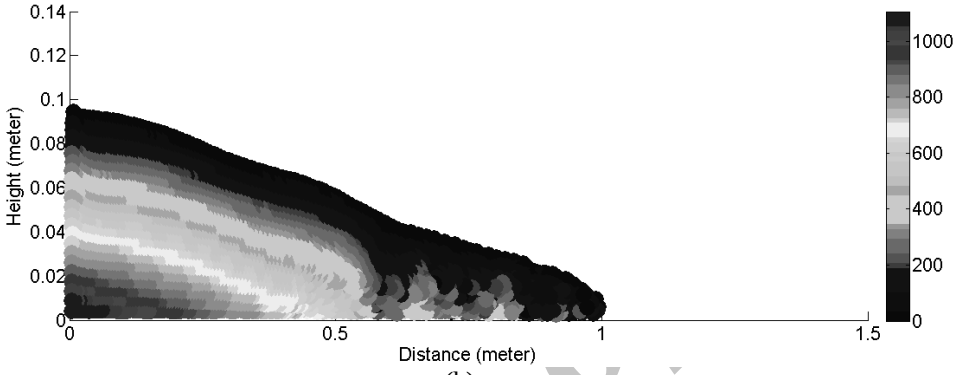

(b)

Fig. 5. Pressure distribution (Pa) after dambreak at times (a) 0.2 s, (b) 0.6 s simulated using ISPH.

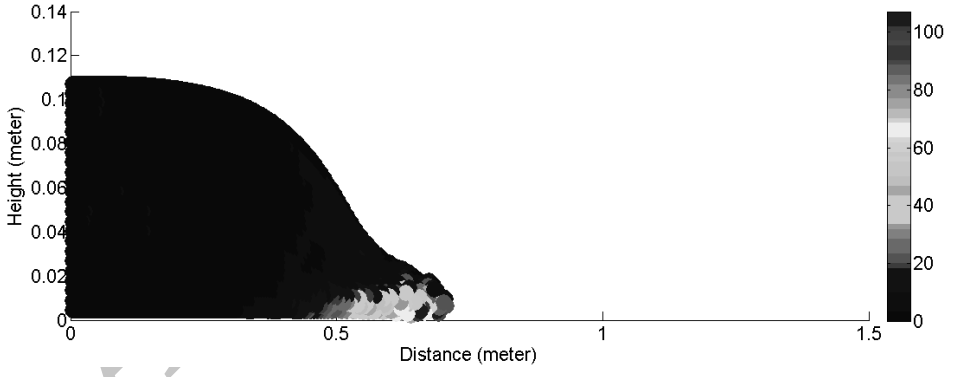

(a)

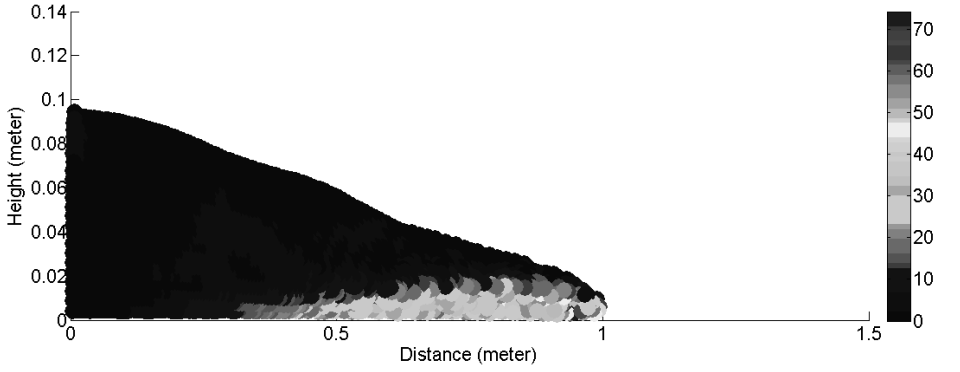

(b)

Fig. 6. Turbulence parameter after dambreak at times (a) 0.2 s, (b) 0.6 s using ISPH

The numerical error was calculated using Eq. (28), and is shown at various times in Fig. 7. The error decreases with time and approaches 0.065%.

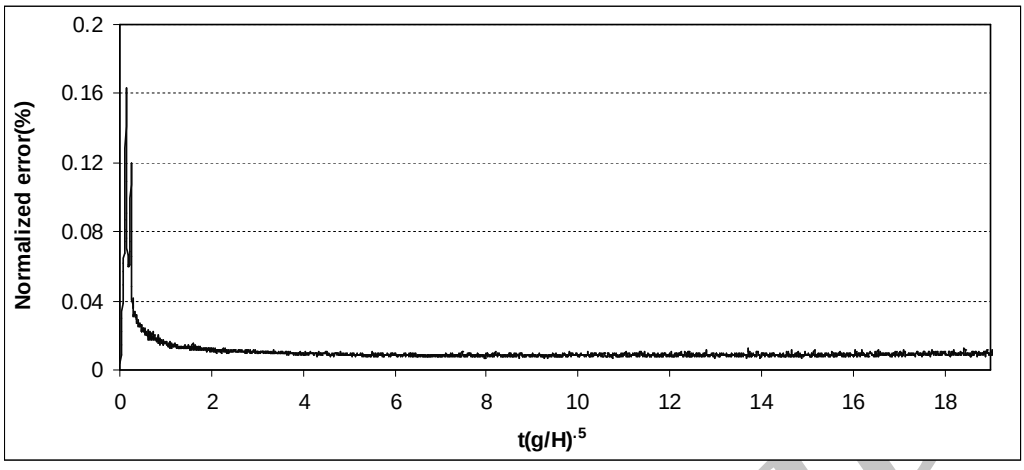

Fig. 7. Error estimated during dambreak simulation based on Eq. (28)

b) Flow under a gate

Gates are frequently used to control discharge of hydraulic structures. Based on the desired properties, there are different types of gate, such as sluice gates [49] or slide gates which are relevant to this research. In recent years, some mesh-free numerical methods such as SPH have been used to solve mudflow which has passed under gates [27]. In this research, the incompressible SPH method is implemented to find the free surface mudflow passed under a gate. To investigate the influence of downstream flow on the results, two different tail water depths were considered. Finite volume with VOF free surface tracking is used to compare results with ISPH. The mudflow rheological properties are again considered according to Table 1.

A tank with length and height equal to 0.15 m, an opening of 0.031 m, and tail water depth equal to 0.027 m are used for the initial geometry of the first case. It is assumed that the gate is removed instantaneously at t=0. Free surface modeling around the gate at two times is shown in Fig. 8, and has excellent agreement with VOF results. A submerged hydraulic jump after the gate shows that the initial depth of hydraulic jump is smaller than contraction depth after the gate.

Mudflow free surface modeling around a gate for a tailwater depth of 0.012 m second case) is shown in Fig. 9. Due to the low tailwater, the initial depth of the hydraulic jump is greater than the contraction depth and leads to a regular hydraulic jump for mudflow. Again, there is a good agreement between the two methods in Fig. 9.

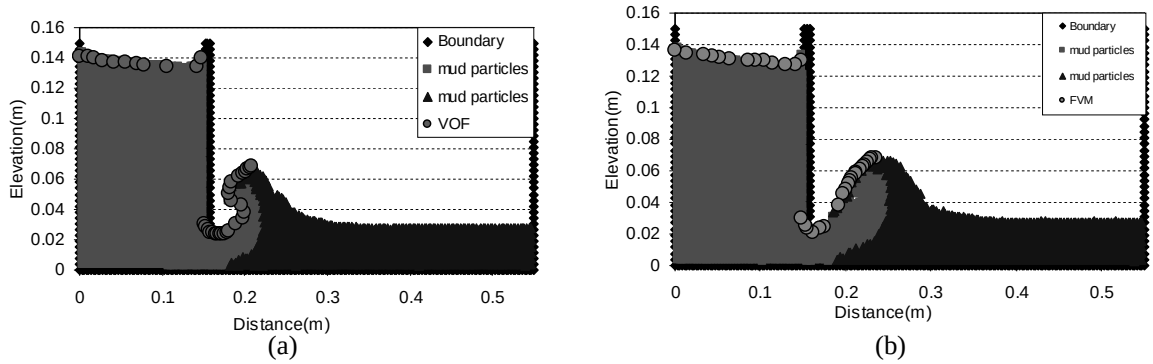

Fig. 8. Free-surface flow after gate for tailwater equal to 0.031 m at times (a) 0.12 s, and (b) 0.19 s using ISPH and FVM-VOF

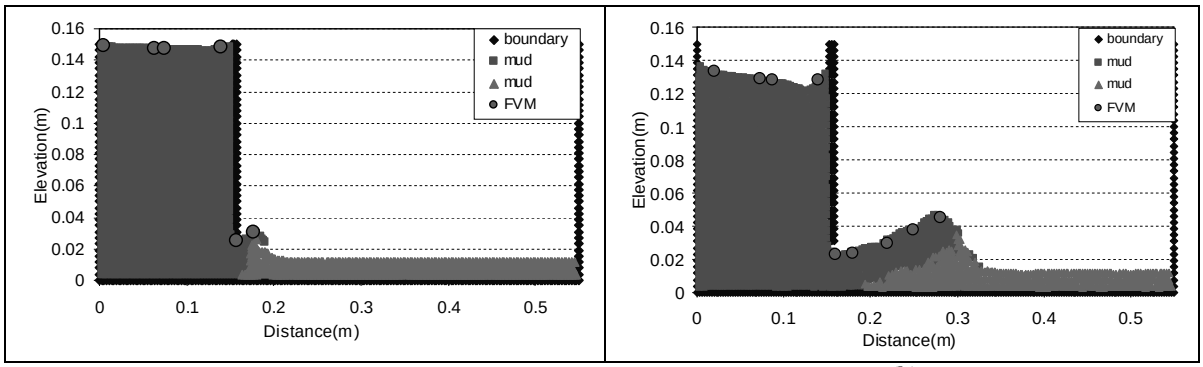

(a) (b)

Fig. 9. Free-surface flow after gate for tailwater equal to 0.031 m at times (a) 0.12 s, and (b) 0.19 s using ISPH and FVM-VOF

To investigate convergence, temporal and spatial intervals are considered 0.001 s and 0.0028 m, respectively. Increasing the length or height of the tank and the number of particles can change the free surface flow to transient or steady situation. Computational characteristics of simulating the flow under the gate for two cases are shown in Table 2. Velocity vectors at two times for the regular and submerged hydraulic jumps are shown in Figs. 10 and 11.

The pressure distribution under the gate at two times for two types of hydraulic jump are shown in Figs. 12 and 13. Near the gate, the distribution deviates from the hydrostatic pressure distribution. However, far from the gate a hydrostatic pressure distribution can be seen.

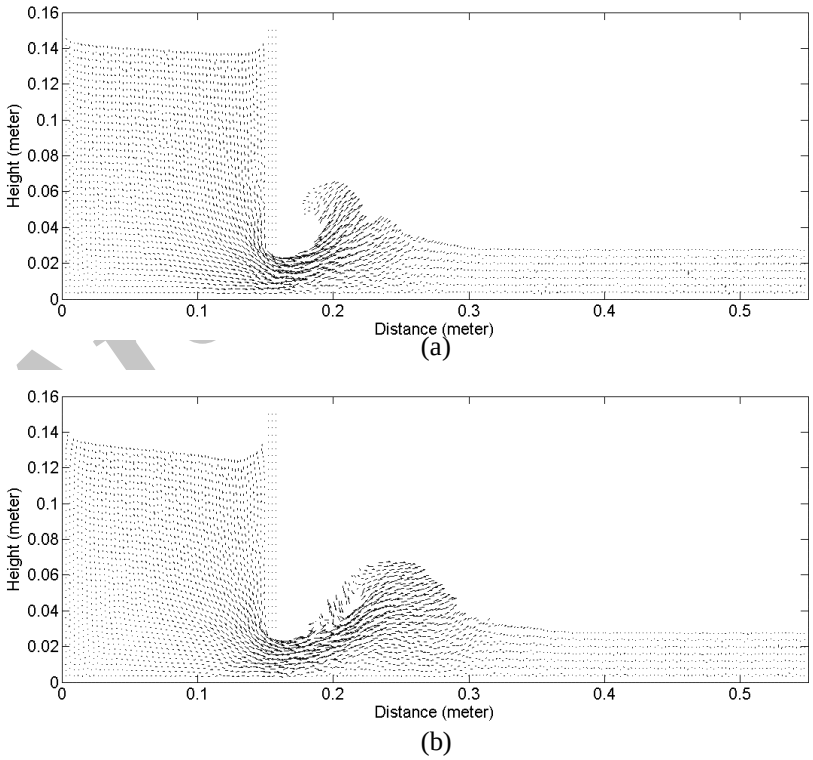

(a)

(b)

Fig. 10. Velocity vector after gate for submerged hydraulic jump at times (a) 0.12 s, (b) 0.19 s using ISPH

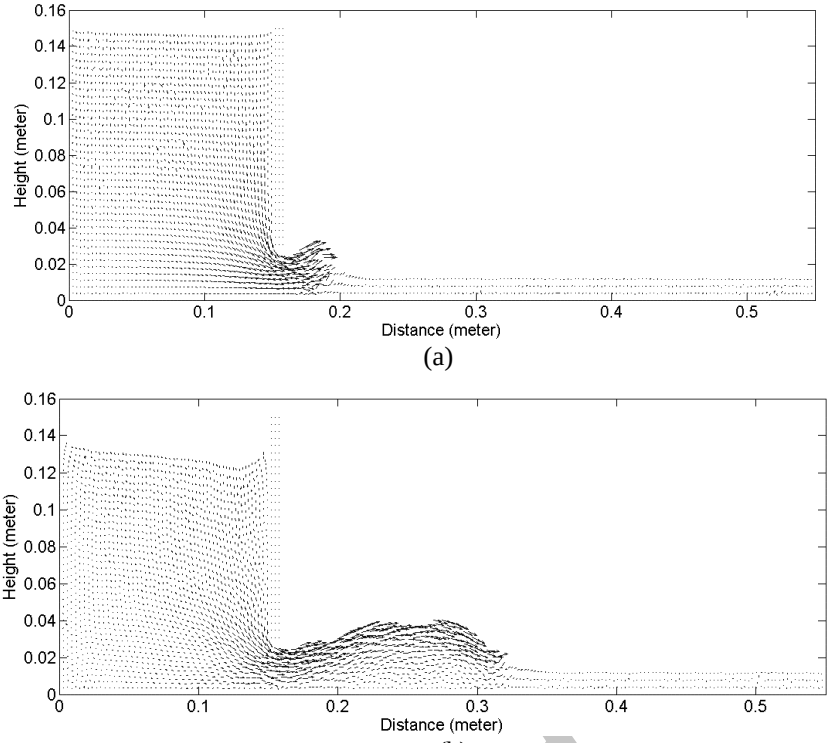

(a)

(b)

Fig. 11. Velocity vector after gate for regular hydraulic jump at times (a) 0.12 s, (b) 0.19 s using ISPH

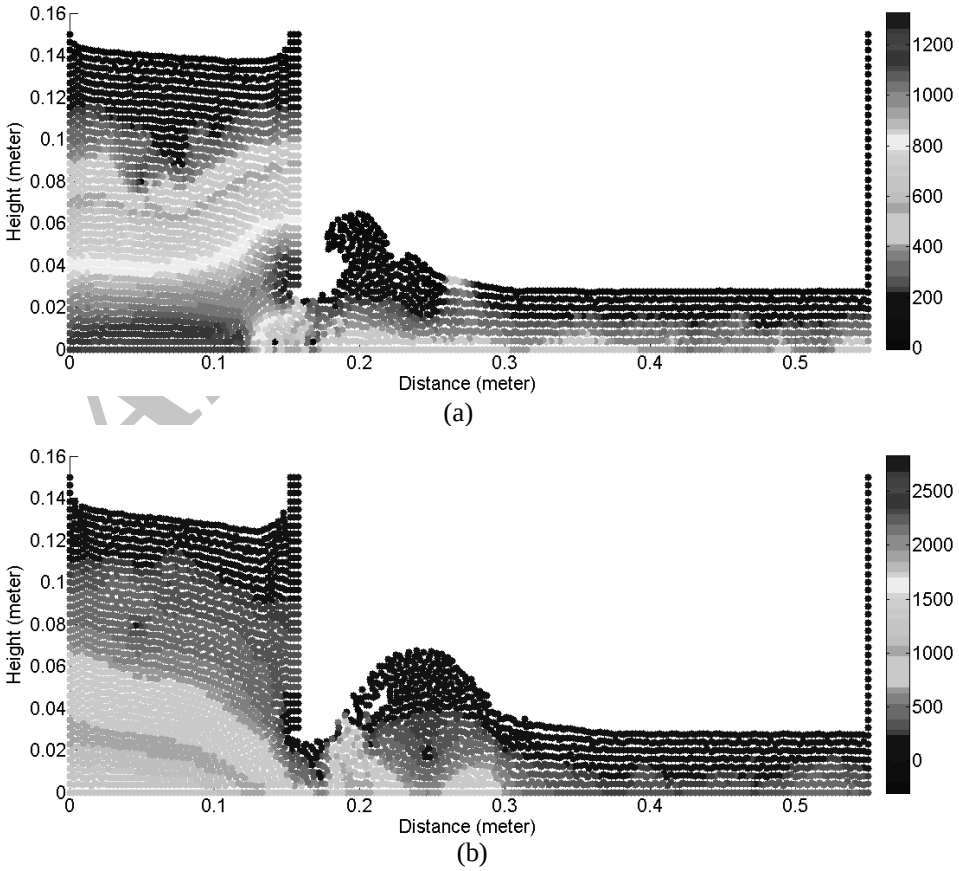

(a)

(b)

Fig. 12. Pressure distribution (Pa) after the gate for submerged hydraulic jump at times (a) 0.12 s, (b) 0.19 s using ISPH

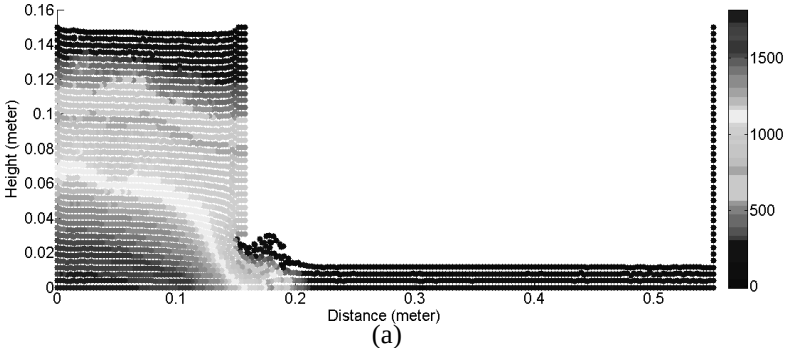

(a)

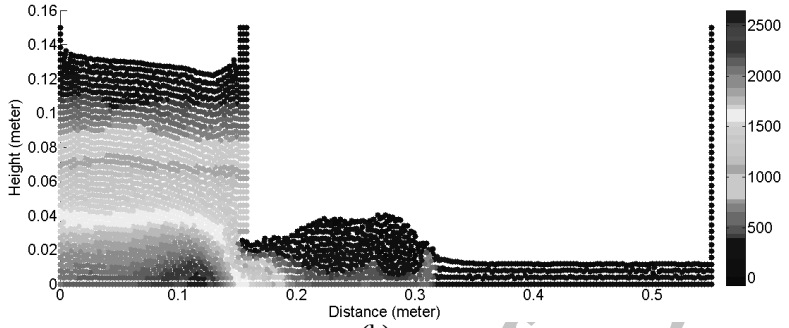

(b)

Fig. 13. Pressure distribution (Pa) after the gate for regular hydraulic jump at times (a) 0.12 s, (b) 0.19 s using ISPH

Turbulence parameter fields (Eq. (8)) at several times for two hydraulic jump examples are shown in Fig. 14 and Fig. 15. The maximum turbulent intensity is near the jump in both cases. Also, the intensity in the submerged hydraulic jump is higher than in the regular hydraulic jump.

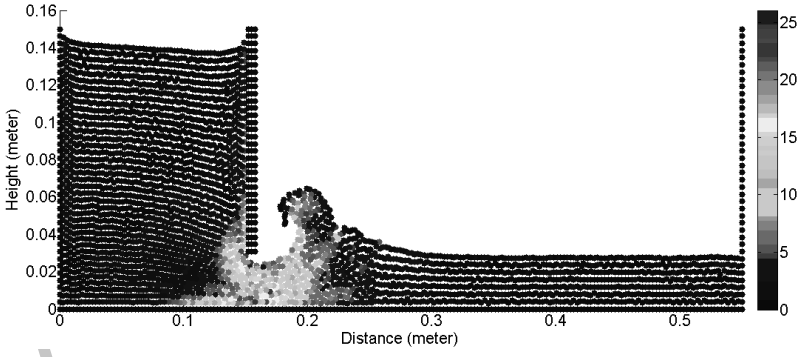

(a)

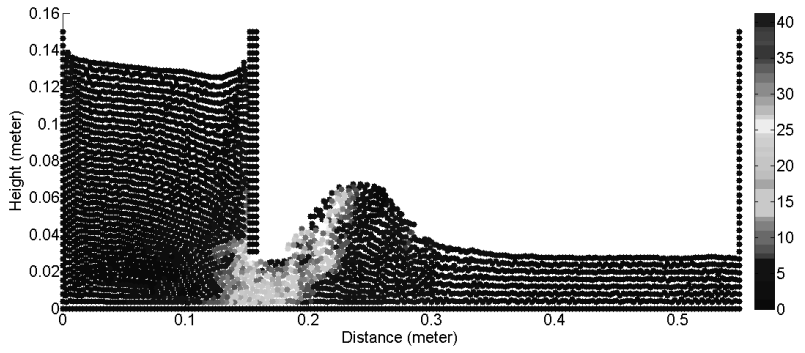

(b)

Fig. 14. Turbulence parameter after the gate (submerged hydraulic jump) at times (a) 0.12 s, (b) 0.19 s using ISPH

The normalized errors calculated using Eq. (28) at various times are shown in Fig.16 for both types of hydraulic jump. After 0.6 and 1.1 s, the error approached 0.15% for the regular and submerged hydraulic jump, respectively.

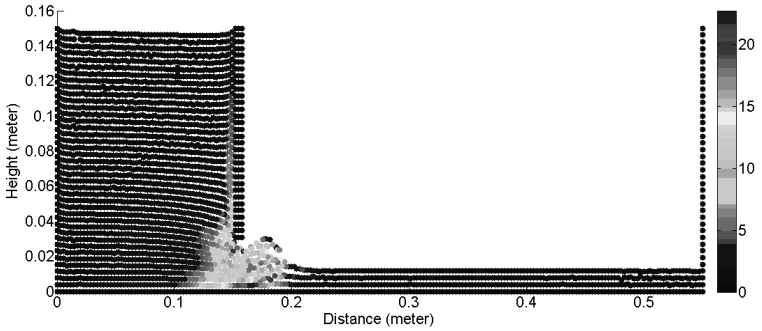

(a)

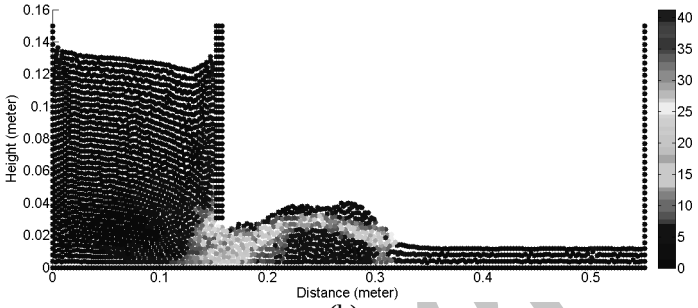

(b)

Fig. 15. Turbulence parameter after the gate (submerged hydraulic jump) at times (a) 0.05 s, (b) 0.19 s using ISPH

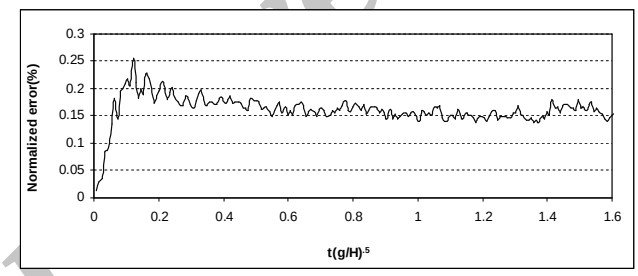

(a)

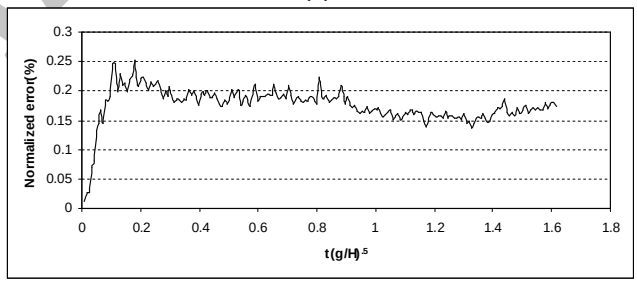

(b)

Fig. 16. Error estimated during (a) regular and (b) submerged hydraulic jump after flow under gate based on Eq. (28)

5. CONCLUSION

ISPH was applied to simulate mudflow in several free surface problems, with the Herschel-Bulkley rheological model used to represent the viscoplastic nature of the mudflow. Results showed that this

numerical technique is capable of handling complex flow cases such as submerged and regular hydraulic jumps after a gate. Further, the multi-phase problem was simulated properly in mudflow gravitational circulation caused by a submarine landslide.

To compare with FVM and other traditional numerical methods, the Lagrangian nature of ISPH makes it very convenient for simulating free surface mudflow in cases with large deformations. The divergence-free velocity projection method properly modeled the incompressibility of mudflow problems, and no violent pressure fluctuations were observed. The maximum error to enforce incompressibility for all of the particles (internal and free surface) was 0.25% for the hydraulic jump problems. We found that for more complicated mudflow problems, larger errors are observed.

According to the rheological parameters of Herschel-Bulkley model ($n \leq \frac{1}{2}$), mudflow has shear-thinning or pseudo-plastic behavior, in which apparent viscosity decreases with increasing shear rate.
The LES turbulence model was applied as a relatively simple model for simulating anisotropic free surface mudflow cases. The maximum turbulent parameter (=70) was observed near the bore front in the dam break case. Also, in the case of flow under a gate, the maximum intensity was located near the impact of the hydraulic jump.

REFERENCES

1. O'Brien, J. S. & Julien, P. Y. (1998). Laboratory analysis of mudflow properties. *Journal of Hydraulic Engineering*, ASCE, Vol. 114, No. 8, pp. 877– 887.
2. Julien, P. Y. & Paris, A. (2010). Mean velocity of mudflows and debris flows. *Journal of Hydraulic Engineering*, ASCE, Vol. 136, No. 9, pp. 676–679.
3. Julien, P. Y. & Lan, Y. Q. (1991). Rheology of hyperconcentrations, *Journal of Hydraulic Engineering*, ASCE, Vol. 117, No. 3, pp. 346–353.
4. Cochard, S. & Ancey, C. (2009). Experimental investigation into the spreading of viscoplastic fluids onto inclined planes, *Journal of Non-Newtonian Fluid Mechanics*, Vol. 158, pp. 73–84.
5. Chambon, G., Ghemmour, A. & Laigle, D. (2009). Gravity-driven surges of viscoplastic fluid: An experimental study. *Journal of Non-Newtonian Fluid Mechanics*, Vol. 158, pp. 54– 62.
6. Laigle, D., Hector, A. F., Hubl, J. & Rickenmann, D. (2003). Comparison of numerical simulation of muddy debris flow spreading to records of real events. URL http://cemadoc.cemagref. fr/cemoa/PUB00012125
7. Shakibaeinia, A. & Jin, Y. C. (2011). A mesh-free particle model for simulation of mobile-bed dam break, *Advances in Water Resources*, Vol. 34, No. 6, pp. 794–807.
8. Cancino, L. & Neves, R. (1999). Hydrodynamic and sediment suspension modelling in estuarine systems Part I: Description of the numerical models. *Journal of Marine Systems*, Vol. 22, pp. 105–116.
9. Chanteperdrix, G., Villediue, P. & Vila, J. P. (2002). A two fluid model for two-phase flows with free interface. *Workshop of Numerical Methods for Multimaterial Compressible Fluid Flows*, Paris.
10. Coussot, P. (1997). *Mudflow rheology and dynamics*. Balkema, Rotterdam.
11. Matson, G. P. & Hogg, A. G. (2007). Two-dimensional dam break flows of Herschel-Bulkley fluids: the approach to the arrested state. *Journal of Non-Newtonian Fluid Mechanics*, Vol. 142, pp. 79–94.
12. Cochard, S. & Ancey, C. (2009). Experimental investigation of the spreading of viscoplastic fluids on inclined planes. *Journal of Non-Newtonian Fluid Mechanics*. Vol. 158, pp. 73–84.
13. Huang, X. & Garcia, M. H. (1997). A perturbation solution for Bingham-plastic Mudflows. *Journal of Hydraulic Engineering*, ASCE, Vol. 123, 11, pp. 986-994.
14. Shao, S. & Lo, E. (2003). Incompressible SPH method for simulating Newtonian and non-Newtonian flows with a free surface. *Advances in Water Resources*, Vol. 26, No. 7, pp. 787–800.
15. Cohard, S. & Ancey, C. (2009). Experimental investigation of the spreading of viscoplastic fluids on inclined plane, *Journal of Non-Newtonian Fluid Mechanics*, Vol. 158, pp. 73–84.

16. Liu, G. & Liu, M. (2003). Smoothed particle hydrodynamics - a meshfree particle method. World Scientific, Singapore, 2003.
17. Liu, M., Liu, G. & Zong, Z. (2008). An overview on smoothed particle hydrodynamics. *International Journal of Computational Methods*, Vol. 5, No. 1, pp.135–188.
18. Lucy, L. (1977). A numerical approach to the testing of fusion process. *Astronomical Journal*, Vol. 88, pp. 1013–1024.
19. Gingold, R. & Monaghan, J. (1977). Smoothed particle hydrodynamics: theory and application to non-SPHerical stars. *Monthly Notices Royal Astronomical Society*, Vol. 181, pp. 375–389.
20. Libersky, L., Petschek, A., Carney, T., Hipp, J. & Allahdadi, F. (1993). High strain lagrangian hydrodynamics a three-dimensional SPH code for dynamic material response. *Journal of Computational Physics*, Vol. 109, No. 1, pp. 67–75.
21. Monaghan, J. (1994). Simulating free surface flows with SPH. *Journal of Computational Physics*, Vol. 110, No. 2, pp. 399–406.
22. Laigle, D., Lachamp, P. & Naaim, M. (2007). SPH-based numerical investigation of mudflow and other complex fluid flow interactions with structures. *Journal of Computers and Geosciences*, Vol. 11, pp. 297–306.
23. Rodriguez-Paz, M. X. & Bonet, J. (2004). A corrected smooth particle hydrodynamics method for the simulation of debris flows. *Numerical Methods for Partial Differential Equations*, Vol. 20, No. 1, pp. 140–163.
24. Shao, S. D. (2010). Incompressible SPH flow model for wave interactions over porous media. *Coastal Engineering*, Vol. 57, No. 3, pp. 304–316.
25. Manenti, S., Di Monaco, A., Agate, G., Gallati, M., Guandalini, R., Maffio, A. & Sibilla, S. (2009). Simulating rapid sediment scour by water flow with SPH. *Proc. 4th SPHERIC Int. Workshop* (France), pp. 144-148.
26. Shao, S. D. (2012). Incompressible smoothed particle hydrodynamics simulation of multifluid flows. *International Journal for Numerical Methods in Fluids*, Doi:10.1002/fld.2660.
27. Chambon, G., Bouvarel, R., Laigle, D. & Naaim, M. (2011). Numerical simulations of granular free-surface flows using smoothed particle hydrodynamics. *Journal of Non-Newtonian Fluid Mechanics*, Vol. 166, pp. 698–712.
28. Mirmohammadi, A. & Ketabdari, M. J. (2011). Numerical simulation of wave scouring beneath marine pipeline using smoothed particle hydrodynamics. *International Journal of Sediment Research*, Vol. 26, No. 3, pp. 331–342.
29. Lee, E. S., Moulinec, C., Xu, R., Violeau, D., Laurence, D. & Stansby, P. (2008). Comparisons of weakly compressible and truly incompressible algorithms for the SPH mesh free particle method. *Journal of Computational Physics*, Vol. 227, No. 18, pp. 8417–8436.
30. Xu, R., Stansby, P. & Laurence, D. (2009). Accuracy and stability in incompressible SPH (ISPH) based on the projection method and a new approach. *Journal of Computational Physics*, Vol. 228, No. 18, pp. 6703–6725.
31. Monaghan, J. (2000). SPH without a tensile instability. *Journal of Computational Physics*, Vol. 159, No. 2, pp. 290–311.
32. Cummins, S. & Rudman, M. (1999). An SPH projection method. *Journal of Computational Physics*, Vol. 152, No. 2, pp. 584–607.
33. Lo, E. & Shao, S. (2002). Simulation of near-shore solitary wave mechanics by an incompressible SPH method. *Applied Ocean Research*, Vol. 24, 5, pp. 275–286.
34. Robinson, M. & Monaghan, J. J. (2011). Direct numerical simulation of decaying two-dimensional turbulence in a no-slip square box using smoothed particle hydrodynamics. *International Journal of Numerical Methods in Fluids*, Doi: 10.1002/fld.2677.
35. Violeau, D., Piccon, S. & Chabard, J. P. (2002). Two attempts of turbulence modelling in smoothed particle hydrodynamics. *Proceedings of the 8th Symposium on Flow Modelling and Turbulence Measurements*. Advances in Fluid Modelling and Turbulence Measurements. World Scientific: Singapore, pp. 339–346.

36. Shao, S. D. (2006). Simulation of breaking wave by SPH method coupled with k–ε model. *Journal of Hydraulic Research*, Vol. 44, 3, pp. 338–349.
37. Violeau, D. & Issa, R. (2007). Numerical modelling of complex turbulent free-surface flows with the SPH method: an overview. *International Journal of Numerical Methods in Fluids*, Vol. 53, pp. 277–304.
38. Shao, S. D. & Gotoh, H. (2005). Turbulence particle models for tracking free surfaces. *Journal of Hydraulic Research*, Vol. 43, No. 3, pp. 276–289.
39. Dalrymple, R. & Rogers, B. (2006). Numerical modeling of water waves with the SPH method. *Coastal Engineering*, Vol. 53, pp. 141–147.
40. Shao, S. D. & Gotoh, H. (2004). Simulating coupled motion of progressive wave and floating curtain wall by SPH-LES model. *Journal of Coastal Engineering*, Vol. 46, pp. 171–202.
41. Shao, J. R., Li, H. Q., Liu, G. R. & Liu, M. B. (2012). An improved SPH method for modeling liquid sloshing dynamics. *Computers and Structures*, Vols. 100-101, pp. 18–26
42. Issa, R., Violeau, D. & Laurence, D. (2005). A first attempt to adapt 3d large eddy simulation to the smoothed particle hydrodynamics gridless method.
43. Chorin, A. (1968). Numerical solution of the Navier-Stokes equations. *Journal of Mathematical Computation*, Vol. 22, pp. 745–762.
44. Liu, M. & Liu, G. (2010). Smoothed particle hydrodynamics (SPH): An overview and recent developments. *Archives of Computational Methods in Engineering*, Vol. 17, No. 1, pp. 25–76.
45. Barnes, H. A. (2000). *A handbook of elementary rheology*. Institute of Non-Newtonian Fluid Mechanics, University of Wales, Aberystwyth, U.K.
46. Zolghadr, M., Hashemi, M. R. & Zomorodian, M. A. (2011). Assessment of Mike21 model in dam and dike-break simulation. *Irainian Journal of Science and Technology, Transactions of Civil Engineering*, Vol. 35, No. C2, pp. 247-262.
47. Ritter. Die fortpflanzung der wasserwellen (in German). (1892). *Vereine Deustcher Ingenieure Zeitwchrift*, Vol. 36, pp. 947-954.
48. Komatina, D. & Jovanovic, M. (1997). Experimental study of steady and unsteady free surface flows with water–clay mixtures. *Journal of Hydraulic Research*, Vol. 35, No. 5, pp. 579– 590.
49. Petrila, T. (2002). Mathematical model for the free surface flow under sluice gate. *Applied Mathematics and Computation*, Vol. 125, pp. 49– 58.